JPET Fast Forward. Published on April 19, 2006 as DOI: 10.1124/jpet.106.102921

ROLE OF PI3 KINASE/AKT AS A SURVIVAL PATHWAY AGAINST CYP2E1 DEPENDENT TOXICITY.

Andres A. Caro and Arthur I. Cederbaum

Department of Pharmacology and Biological Chemistry, Mount Sinai School of Medicine, New York, NY 10029, USA. (AAC, AIC)

Running title: PI3 kinase/AKT and CYP2E1 toxicity.

Address correspondence to: Andres A. Caro, Department of Pharmacology and Biological Chemistry, Box 1603, Mount Sinai School of Medicine, One Gustave L. Levy Place, New York, NY 10029, USA. Telephone: (212) 241-7285; Fax: (212) 996-7214; E-mail: Andres.Caro@mssm.edu

Number of text pages: 44

Number of tables: 1

Number of figures: 9

Number of references: 40

Number of words in the Abstract: 250

Number of words in the Introduction: 614

Number of words in the Discussion: 1215

Abbreviations: ROS, reactive oxygen species; MTT, 3 [4,5-dimethylthiazol-2-yl] 2,5-diphenyltetrazolium bromide; TBARS, thiobarbituric acid reactive substances; DCFH-DA, 2'7'-dichlorofluorescein diacetate; Fe-NTA, iron-nitrilotriacetate 1:3 complex; E47 cells, HepG2 cell line derived after transfection with pCI-neo vector containing the human CYP2E1 cDNA; C34 cells, HepG2 cell line derived after transfection with pCI-neo vector; MEM_{exps}, MEM medium supplemented with 5% fetal bovine serum and 100 units/mL of penicillin and 100 μg/mL of streptomycin; ADV-MyrAKT, adenovirus expressing a constitutively active form of AKT tagged with the hemagglutinin epitope under the control of the cytomegalovirus promoter; ADV-LacZ, adenovirus expressing β-galactosidase under the control of the cytomegalovirus promoter; 7-MFC, 7-methoxy-4-trifluoromethylcoumarin; MPT, mitochondrial permeability transition.

Recommended Section: Cellular and Molecular

ABSTRACT

The objective of this work was to evaluate the possible role of PI3 kinase /AKT as a survival pathway against CYP2E1-dependent toxicity. E47 cells (HepG2 cells transfected with human CYP2E1 cDNA) exposed to 25 μM Fe-NTA + 5 μM arachidonic acid (AA+Fe) developed higher toxicity than C34 cells (HepG2 cells transfected with empty plasmid). Toxicity was associated with increased oxidative stress, and activation of calcium-dependent hydrolases calpain and phospholipase A2 (PLA2). Treatment of E47, but not C34 cells, with AA+Fe led to a decrease in the phosphorylation state of AKT. LY294002, a specific inhibitor of PI3 kinase, produced a further decrease of phosphorylated AKT in AA+Fe-treated E47 cells. LY294002 and down regulation of endogenous AKT with siRNAs increased the toxicity of AA+Fe in E47 cells. Toxicity of AA+Fe in rat hepatocytes was also increased by LY294002. LY294002 did not affect PLA2 or calpain activation, CYP2E1 activity, or lipid peroxidation elicited by AA+Fe. α-Tocopherol prevented both AA+Fe and AA+Fe+LY294002-induced toxicity and decrease of phosphorylated AKT. LY294002 potentiated AA+Fe-induced loss of mitochondrial membrane potential and ATP, while overexpression of constitutively active AKT partially prevented mitochondrial impairment and toxicity. Mitochondrial permeability transition inhibitors prevented both AA+Fe and AA+Fe+LY294002-induced toxicity and decrease of mitochondrial membrane potential. These results suggest: i) AA+Fe+CYP2E1-induced oxidative stress decreases AKT activation; ii) AKT inactivation induces mitochondrial impairment associated with opening of the permeability transition pore but not dependent on the activation state of bad, GSK-3β, mTOR or bcl-xl; iii) PI3 kinase/AKT may serve as a survival pathway against CYP2E1 dependent toxicity.

INTRODUCTION

Recent data have implicated phosphatidylinositol 3-kinase (PI3 kinase) and their phospholipid products in promoting cell survival downstream of extracellular stimuli (Datta et al., 1999). Briefly, PI3 kinase converts the plasma membrane lipid phosphatidylinositol-4,5-bisphosphate ($PI(4,5)P_2$) to phosphatidylinositol-3,4,5-trisphosphate ($PI(3,4,5)P_3$). AKT and PDK1 directly bind to $PI(3,4,5)P_3$ through their pleckstrin-homology domain. This association at the membrane brings these proteins into proximity and facilitates phosphorylation of AKT by PDK1, which activates AKT, resulting in the phosphorylation (and subsequent inhibition) of several targets that affect cell survival (Cantley, 2002).

In liver cells, activation of PI3 kinase/AKT is the principal pathway through which many molecules exert their antiapoptotic effect. EGF inhibits apoptosis mediated by choline deficiency through PI3K/AKT activation (Albright et al., 2005), and the same occurs for insulin (Bilodeau et al., 2004), HGF (Schulze-Bergkamen et al., 2004), lysophosphatidic acid (Sautin et al., 2001), and IL-6 (Kuo et al., 2001), which inhibit apoptosis mediated by TGF–β, CD95, TNF-α/galactosamine, and retinoic acid, respectively, through PI3K/AKT activation. Furthermore, other agents promote liver cell apoptosis through suppression of PI3 kinase/AKT: sphingosine (Chang et al., 2001), celecoxib (Leng et al., 2003) and FTY720 (Lee et al., 2004). Several targets of the PI3 kinase AKT/pathway may underlie the ability of this regulatory cascade to promote survival, including bad, caspase 9, transcription factors of the forkhead family, IKK which regulates NF-κB, and GSK-3β (Datta et al., 1999). There is more limited experimental evidence for the role of PI3 kinase/AKT in the protection against liver necrosis. The expression of myrAKT reduces hepatocyte necrosis in the rat liver central vein following ischemia/reperfusion (Harada et al., 2004). Ischemic preconditioning decreases the number of necrotic and apoptotic

liver cells after ischemia/reperfusion, through activation of AKT (Izuishi et al., 2003). Loss of all isoforms of PI3 kinase p85α results in perinatal lethality in knock-out mice, characterized by extensive hepatocyte necrosis (Fruman et al., 2000).

In liver cells, oxidative stress-promoting conditions such as sulfur aminoacid deprivation (Kang et al., 2001a) tert-butylhydroquinone (Kang et al., 2001b) and ischemia-reperfusion (Harada et al., 2004) activate PI3-kinase and AKT. Following oxidative stress conditions in liver cells, activation of PI3 kinase/AKT was responsible for the induction of rGSTA2 mediated by the antioxidant response element (Kang et al., 2001b), for the induction of microsomal epoxide hydrolase (Kang et al., 2001a), and for increased phosphorylation of bad and decreased release of cytochrome c (Harada et al., 2004), events associated with protection against injury.

Microsomes represent a potential source of reactive oxygen species (ROS) via cytochrome P450 (Zangar et al., 2004). In comparison with other isoforms of cytochrome P450, CYP2E1 exhibits increased NADPH oxidation and capacity to induce ROS and lipid peroxidation. CYP2E1 overexpression in HepG2 cells and primary rat liver cells is associated with increased cytotoxicity of arachidonic acid (AA), glutathione (GSH) depletion, iron-nitrilotriacetate (Fe-NTA) and ethanol. Increased production of ROS is a main cause of the increased cytotoxicity, which was associated with increased lipid peroxidation and early intracellular 2',7'-dichlorofluorescein diacetate (DCFH-DA) oxidation, and was inhibited by antioxidants. Toxicity in these models show morphological and biochemical features of necrosis and apoptosis, depending on the nature of the insult (Caro and Cederbaum, 2004).

Considering the role of the PI3 kinase/AKT pathway in liver cell survival, in particular following oxidative stress, and the cellular toxicity caused by overexpression of CYP2E1 in liver cells, the objectives of this work were: i) to evaluate possible changes in AKT levels and activation after

exposure of HepG2 cells overexpressing CYP2E1 to AA+Fe-NTA, an oxidative stress- and CYP2E1-dependent toxicity model that is mainly necrotic in nature; ii) to evaluate a possible role of PI3 kinase/AKT in the protection of liver cells against CYP2E1-dependent necrosis; iii) to study possible mechanisms involved in the effects of PI3 kinase/AKT.

MATERIALS AND METHODS

Chemicals: Phosphate buffered saline (PBS) was from Roche (Newark, NJ). G418 was from Invitrogen (Carlsbad, CA). Fluo3-AM and pluronic acid were from Molecular Probes (Eugene, OR). ^{3}H-AA was from Perkin Elmer (Boston, MA). Protein concentration was measured using the BioRad DC Protein assay (Hercules, CA). Most other chemicals used were from Sigma Chemical Company (St Louis, MO). Antibodies for inmunoblots were from Santa Cruz (Santa Cruz, CA) except for anti-spectrin which was from Chemicon (Temecula, CA). siRNAs against AKT1, 2 and 3 were purchased from New England Biolabs (Beverly, MA), and siRNA transfection reagent DharmaFect 1 was from Dharmacon (Lafayette, CO).

Culture and treatment of cells: Two human hepatoma HepG2 cell lines described in Chen and Cederbaum (1998), were used as models in this study: E47 cells, which constitutively express human CYP2E1, and C34 cells, which are HepG2 cells transfected with the empty pCI vector. Both cell lines were grown in minimal essential medium Eagle (MEM) containing 10% fetal bovine serum and 0.5 mg/mL of G418 supplemented with 100 units/mL of penicillin and 100 μg/mL of streptomycin, in a humidified atmosphere in 5% CO_2 at 37°C. Cells were subcultured at a 1:5 ratio once a week. For the experiments, cells were plated at a density of 50000 cells/mL and incubated for 12 h, in MEM supplemented with 5% fetal bovine serum and 100 units/mL of penicillin and 100 μg/mL of streptomycin (MEM_{exps}). After this period, the medium was replaced with MEM_{exps} supplemented with AA (from 0 to 5 μM). After 12 h of incubation at 37 °C, the medium was removed and the cells were washed once with PBS to remove unincorporated arachidonic acid. The cells were incubated for an additional 12 h period with MEM_{exps}. Then, the medium was supplemented with various additions (e.g. antioxidants, inhibitors) for 1h, prior to the addition of buffer or Fe-NTA (25 μM), which was considered as

the initiation of the cellular toxicity phase (time= 0h). The cells were incubated for variable periods (up to 3h) before the biochemical analyses. This basic protocol, i.e., preloading with arachidonic acid, washing, adding inhibitors, and initiating the toxicity phase by addition of Fe-NTA, was used for all experiments (Caro and Cederbaum, 2001).

Selected experiments were carried out using primary hepatocyes from male Sprague-Dawley rats purchased from In Vitro Technologies (Baltimore, MD). In this case, rat hepatocyes were plated on MEM_{exps} at a density of 30000 cells/mL, and after 6h, AA was added (0-25 μM) for 12h. After this, cells were washed once with PBS, MEM_{exps} was added, followed by a 1h preincubation with inhibitors. This was followed by addition of Fe-NTA for 6h, after which biochemical analyses were performed on the cells.

Measurement of phospholipase A2 (PLA2) activity in situ: PLA2 activation was monitored in cultured cells using tritiated arachidonic acid as previously described (Caro and Cederbaum, 2003). 50000 cells were plated onto 24 well plates in MEM_{exps}. Cells were first incubated with 2 μM AA and labeled with 0.2 μCi/ml ^{3}H-AA, in MEM_{exps} for 12h. Cells were washed with PBS, and incubated with MEM_{exps} for an additional 12h-period. After this, the cells were washed 4 times with PLA2 assay buffer: PBS pH 7.2 supplemented with 5.5 mM glucose, 0.8 mM $MgSO_4$, 0.1% fatty acid free BSA and 1 mM $CaCl_2$. 500 μl of this PLA2 assay buffer at 37 °C was added per well. Cells were put in a shallow water bath at 37 °C for 15 min, to allow equilibration of the cells. Then, where indicated, inhibitors were added, and the cells incubated for 1h. After this time, buffer or Fe-NTA (25 μM) was added, and ^{3}H-AA release was evaluated after 2h. To evaluate ^{3}H-AA release, the medium containing the released ^{3}H-AA was removed, placed in eppendorf tubes and centrifuged for 2 min at 5000 rpm. The supernatant was transferred to scintillation vials and the pellet containing detached cells was kept. The cells in each well were

JPET Fast Forward. Published on April 19, 2006 as DOI: 10.1124/jpet.106.102921
This article has not been copyedited and formatted. The final version may differ from this version.

resuspended by adding 500 µl of 0.1% Triton X-100. The content of each well was transferred to the eppendorf tubes containing the corresponding cellular pellet, and vortexed. Finally, the suspension was transferred to scintillation vials. 4 ml of scintillation fluid was added to each vial, and after vigorously shaking, the radioactive content was determined by scintillation counting using a β-counter. The data were expressed as percentage of cellular ^{3}H-AA released: 100x[^{3}H-AA released/(^{3}H-AA incorporated+^{3}H-AA released)]. Validation of this method and evidence that the released radioactivity was indeed ^{3}H-AA was previously studied (Caro and Cederbaum, 2003).

Cytotoxicity measurements: 5 x 10^4 cells were plated onto 24 well plates and after the corresponding treatment, the medium was removed, and cell viability was evaluated by the MTT test (Caro and Cederbaum, 2003).

Measurement of intracellular calcium: The intracellular calcium levels were determined with the fluorescent calcium indicator fluo3-AM by flow cytometry. 5x 10^5 cells were plated in 10 mm-Petri dishes and at the end of the various treatments the medium was replaced with 3 mL of MEM_{exps} without fetal bovine serum plus 2.5 µM fluo3-AM and 0.02% pluronic acid (stock solution x1000 in DMSO). Cells were incubated for 30 min at 37°C. After loading, the cells were washed in PBS (to remove any dye non-specifically associated with the cell surface), trypsinized, and resuspended in 1 mL of MEM_{exps} without fetal bovine serum plus 5 µg of propidium iodide (PI). PI was used to assay for the viable cell population as these cells exclude this dye, whereas non-viable cells take up this dye. The measurement of $[Ca^{2+}]_i$ was performed by flow cytometry analysis of 5000 cells using Cell Quest software. Intracellular calcium level was evaluated as Fluo3 fluorescence intensity in PI negative (i.e. viable) cells (Caro and Cederbaum, 2003). 10 µM ionomycin was applied to one sample before each experiment to check for correct loading of

the cells and thus served as a positive control. The inhibitors tested did not interfere with the quantification of the fluorescence (488/525 nm excitation/emission) of a standard fluo3-Ca^{2+} solution.

Lipid peroxidation assay: The production of thiobarbituric acid-reactive substances (TBARS) was assayed as previously described (Caro and Cederbaum, 2001). The protein concentration of the cell suspension was determined using a protein assay kit based on the Lowry assay (BioRad DC kit). The concentration of malondialdehyde was calculated from a standard curve prepared using malonaldehyde bisdimethylacetal.

CYP2E1 activity in intact cells: Incubations (in duplicate) were performed using 1 millon E47 cells/mL of MEM without phenol red and fetal bovine serum, at 37 °C in a CO_2 incubator. Reactions were initiated by the addition of 100 μM 7-methoxy-4-trifluoromethylcoumarin (7-MFC) (stock solution 500x in acetonitrile), and after 0-2 h, cells were scraped and fluorescence of the suspension was determined at 409/530 nm (Ghosal et al., 2003).

Flow cytometry analysis of the mitochondrial membrane potential: The mitochondrial transmembrane potential was analyzed from the accumulation of rhodamine 123, a membrane-permeable cationic fluorescent dye. Cells were plated onto 6 well plates, and at the end of the treatment the medium was replaced with fetal bovine serum-free MEM_{exps} containing 5 μg/mL rhodamine 123, and incubated at 37 °C for 1 h. The cells were then harvested by trypsinization, washed with PBS, and resuspended in 1 mL of fetal bovine serum-free MEM_{exps} containing 5 μg/mL PI. The intensity of fluorescence from rhodamine 123 and PI was determined using a BD FACSCalibur Flow Cytometer (San Jose, CA) as previously described (Caro and Cederbaum, 2001).

JPET Fast Forward. Published on April 19, 2006 as DOI: 10.1124/jpet.106.102921
This article has not been copyedited and formatted. The final version may differ from this version.

ATP content: The ATP content was determined by the luciferin-luciferase method. Cells were plated onto 6 well plates, and after the corresponding treatment, harvested by trypsinization. The cells were washed twice with PBS, and resuspended in the same buffer. An aliquot of the cell suspension was assayed for ATP using the SIGMA Chemical Luciferase ATP assay kit. The amount of ATP in experimental samples was calculated from a standard curve prepared with ATP, and expressed as nmol/mg protein. The protein concentration in the cellular suspension was determined as previously described.

Intracellular ROS measurement: Intracellular ROS production was monitored with DCFH-DA as the probe. 3×10^5 cells were plated in 10-mm Petri dishes, and after the corresponding treatment, the medium was replaced with FBS-free MEM_{exps} supplemented with 10 µM DCFH-DA. The cells were incubated for 30 min at 37 °C, and after this incubation, they were washed with PBS, trypsinized, and resuspended in 1 mL of FBS-free MEM_{exps} plus 5 µg of PI. 5000 cells were analyzed by flow cytometry using Cell Quest software.

Determination of GSH levels: After treatment, the cells were washed twice with PBS, detached by trypsinization, and treated with 10% (1:1, v/v) trichloroacetic acid to extract cellular GSH. The mixture was centrifuged at 13,000 × *g* for 1 min to remove denatured proteins, and GSH was determined by the enzymatic method of Tietze (Tietze, 1969). The total GSH content was assayed by following the increase in absorbance at 412 nm for 2 min in a cuvette containing 0.1 M sodium phosphate buffer (pH 7.5), 5 µM EDTA, 0.6 mM 5,5'-dithiobis(2-nitrobenzoic acid), 0.2 mM NADPH, 10 U/mL glutathione reductase, and 20 µL of sample (corresponding to ~50 µg of protein) in a final volume of 1 mL.

Western blots: After washing the cells with PBS, cells were incubated on ice for 15 min in extraction buffer (250 mM Tris-HCl, pH 8.0, 150 mM NaCl and 1% IGEPAL CA-630)

containing 1 mM sodium orthovanadate, 50 μg/mL aprotinin and 0.1 mg/mL PMSF. Lysates were centrifuged at 15000 rpm at 4°C to remove insoluble material, and the protein concentration in whole cell lysates was measured using the BioRad DC protein assay kit. Protein samples (30 μg) were separated by SDS-PAGE, transferred to nitrocellulose membranes, and incubated with primary and secondary antibodies. Antibodies were used at the following dilutions: anti-phospho-AKT (Thr308) (1:1000), anti-AKT (1:1000), anti-phospho-bad (Ser136) (1:200), anti-bad (1:100), anti-bcl-xL (1:250), anti-β-actin (1:10000), anti-spectrin (1:1000), anti-phospho-GSK3β (Ser9) (1:1000), anti-GSK-3β (1:1000), anti-phospho-mTOR (Ser2448) (1:1000), and anti-mTOR (1:1000).

Adenovirus infection: Adenovirus vectors expressing constitutively active forms of AKT tagged with the hemagglutinin epitope (ADV-MyrAKT), or β-galactosidase (ADV-LacZ) under the control of the cytomegalovirus promoter, were obtained from Vector Biolabs (Philadelphia, PA). The constitutively active AKT has the c-Src myristoylation sequence fused in frame to the N terminus of the wild type AKT coding sequence that targets the fusion protein to the membrane. Cells destined to be infected were first loaded with AA following the standard protocol (12h incubation with 5 μM AA or FBS in the case of controls, wash with PBS, and 12h incubation with MEM_{exps}). For infection, recombinant adenovirus was diluted in MEM containing 2% fetal bovine serum, and added to the cells at 37 °C for 1h. After addition of an equal volume of MEM with 10% fetal bovine serum, cells were incubated for an additional 5h period. After this, the medium was replaced with MEM_{exps}, and the cells incubated for 18h, followed by the addition of Fe-NTA (or buffer in the case of controls). Recombinant adenoviruses were used at a multiplicity of infection of 10.

Statistics: Data are expressed as mean ± standard error of the mean from 3 to 4 independent experiments run in duplicate. One-way analysis of variance (ANOVA) with subsequent post hoc comparisons by Scheffe was performed. A $p < 0.05$ was considered as statistically significant.

RESULTS

Effect of AA+Fe and inhibition of the PI3 kinase/AKT pathway, on AKT levels and cellular toxicity in CYP2E1-expressing liver cells.

We have previously reported that E47 cells (HepG2 cells transfected with a plasmid encoding the human CYP2E1 cDNA) exposed to 5 μM arachidonic acid + 25 μM Fe-NTA (AA+Fe) showed significant cytotoxicity with respect to C34 cells (HepG2 cells transfected with the empty plasmid, not expressing any cytochrome P450) (Caro and Cederbaum, 2001). The first objective of this work was to investigate if cell death in this CYP2E1- dependent model of cytotoxicity was associated with changes in the levels or activation of AKT. Fig 1A (left panels) shows representative immunoblots for phosphorylated AKT and total AKT in lysates prepared from E47 cells loaded with arachidonic acid, and exposed to iron for 0 to 3h. A time-dependent decrease of phosphorylated AKT levels was observed, while total AKT levels remained relatively constant. These changes are reflected by a significant decrease in the relative ratio of pAKT over total AKT with time (Fig 1A, left panel, numbers in parentheses below the blot). After 3h of incubation with AA+Fe the pAKT/AKT ratio was decreased by 30% compared to the 0h and almost 50% compared to the 3h vehicle control incubation (0.7 vs 1.3). Similar kinetic experiments were done after preincubation with 10 μM LY294002, a specific cell permeable PI3 kinase inhibitor (Fig 1B, left panels). There was also a decrease in phosphorylated AKT with time of incubation with Fe-NTA, and non significant changes in total AKT, but the decrease in phosphorylated AKT was more pronounced than in the absence of LY294002. These changes are reflected by an early and pronounced decrease in the relative ratio of pAKT over total AKT with time (Fig 1B, left panels, numbers in parentheses below the blot). This decrease in pAKT/AKT occurs at time points e.g. 0.5, 1h prior to cell death (discussed below, Fig 2A). Several control

experiments were performed; a) in the presence of the vehicle alone (0.1% DMSO) (Fig 1A, right 2 panels), or in the presence only of 10 μM LY294002 (Fig 1B, right 2 panels), but without AA+Fe, no significant changes in phosphorylated or total AKT were observed after 3h of incubation; b) AA-loaded C34 cells exposed to Fe-NTA did not show significant changes in phosphorylated or total AKT after 3h of incubation with Fe-NTA, either in the absence or presence of 10 μM LY294002 (Fig 1C); and c) LY303511, an inactive analog of LY294002, did not produce significant changes in AKT levels or activation in AA+Fe-treated E47 cells as LY294002 did (data not shown).

E47 cells loaded with 5 μM arachidonic acid and exposed to 25 μM Fe-NTA showed a time-dependent toxicity that started after 1h of exposure to Fe-NTA (Fig 2A). E47 cells exposed similarly to AA+Fe, but preincubated with 10 μM LY294002, showed an increased loss of viability with respect to cells exposed to AA+Fe in the absence of the inhibitor. 10 μM LY294002 was not toxic by itself in these conditions (Fig 2A). E47 cells preincubated with 10 μM of the inactive analog LY303511 and exposed to AA+Fe, did not show a significant change in cellular toxicity with respect to AA+Fe-treated cells (data not shown). AA+Fe added to C34 cells did not produce significant toxicity (Fig 2B). C34 cells preincubated with 10 μM LY294002 and exposed to AA+Fe showed a small increase in cellular toxicity with respect to C34 cells exposed to AA+Fe in the absence of LY294002 (Fig 2B). However, toxicity in C34 cells exposed to LY294002 and AA+Fe was significantly less than in E47 cells incubated in the same conditions. Other inhibitors of protein kinases such as SB203580 (p38 MAPK inhibitor) and PD98059 (ERK inhibitor) did not increase AA+Fe toxicity in E47 cells (data not shown). Interestingly, SB203580 was previously shown (Wu and Cederbaum, 2003) to inhibit the slowly developing (24-48h) toxicity of AA alone or BSO alone in the E47 cells but not the rapid (1-3h)

JPET Fast Forward. Published on April 19, 2006 as DOI: 10.1124/jpet.106.102921
This article has not been copyedited and formatted. The final version may differ from this version.

toxicity found with AA plus Fe. It appears that different signaling pathways play a role in the toxicity mechanisms in the E47 cells depending of the toxin and time course for development of toxicity. Morphologically, toxicity by AA+Fe in E47 cells was characterized by cell swelling and membrane blebs, vacuolization and cytoplasmic degradation (Fig 2C). In cells preincubated with 10 μM LY294002 and treated with AA+Fe, similar morphological changes were observed, although they were much more pronounced than in the absence of LY294002 (Fig 2C). These experiments suggest that inhibition of the PI3 kinase/AKT pathway potentiates AA+Fe toxicity in the E47 cells.

In the following set of experiments we tested the effect of other inhibitors of the PI3 kinase/AKT pathway, structurally or functionally unrelated to LY294002, on the toxicity of AA+Fe in E47 cells. AKT inhibitor IV is an inhibitor of AKT phosphorylation and activation that targets a kinase downstream of PI3 kinase. AKT inhibitor IV (at 0.5-2 μM) increased the toxicity of AA+Fe without showing significant toxicity by itself (Fig 3A, upper panel). AKT inhibitor IV also lowered the level of phosphorylation of AKT in the presence of AA+Fe without affecting total AKT levels, with respect to E47 cells treated with AA+Fe alone (Fig 3A, lower panel). Deguelin is an inhibitor of PI3 kinase and activated AKT, and in the same way, increased the toxicity of AA+Fe in the concentration range 1-10 μM, without showing significant toxicity by itself (Fig 3B, upper panel). Deguelin also lowered the level of phosphorylation of AKT in the presence of AA+Fe without affecting total AKT levels, with respect to E47 cells treated with AA+Fe alone (Fig 3B, lower panel). Another approach was the use of siRNAs to lower pAKT as well as total AKT levels. E47 cells pre-exposed to a pool of siRNA against AKT1, 2 and 3 during 24h developed higher AA+Fe toxicity than E47 cells pre-exposed to a control, non-targeting siRNA, and treated with AA+Fe (Fig 3C, upper panel). E47 cells pre-exposed to

AKT1/2/3 siRNA and treated with AA+Fe showed a significant decrease of total AKT levels, and a significant decrease of phosphorylated AKT, with respect to cells pre-exposed to a control, non-targeting siRNA and treated with AA+Fe (Fig 3C, lower panel). Thus, use of 3 different chemical inhibitors as well as siRNA show that the PI3 kinase/AKT pathway is protective against AA/Fe toxicity in the E47 cells. On the contrary, wortmannin, also a cell-permeable inhibitor of PI3 kinase, did not show any effect on AA+Fe toxicity, in the concentration range 0.1-10 μM (Fig 3D, upper panel). However, wortmannin did produce a decrease in phosphorylated AKT levels in cells treated with AA+Fe with respect to cells treated with AA+Fe alone, suggesting it is an inhibitor of PI3 kinase in this system (Fig 3D, lower panel). The specificity of wortmannin was evaluated to try to explain the lack of potentiation of AA+Fe toxicity as found with the other PI3 kinase/AKT inhibitors. There is data that wortmannin, at the same range of concentrations where it is an effective inhibitor of PI3 kinase, also effectively inhibits PLA2 (Cross et al., 1995). PLA2 plays a critical role in the toxicity by AA+Fe in E47 cells (Caro and Cederbaum, 2003). PLA2 activity in E47 cells in situ was determined by measuring the release of pre-loaded ^{3}H-AA into the medium. AA+Fe produced an increase in the release of ^{3}H-AA, which was inhibited by a general PLA2 inhibitor, 100 μM quinacrine (Fig 4). Wortmannin (0.1 to 10 μM) inhibited both the basal release of ^{3}H-AA, and the increased release of ^{3}H-AA after treatment with AA+Fe. This suggests that in our system wortmannin acts both as a PI3 kinase and a PLA2 inhibitor. While the former should potentiate toxicity, the latter blocks toxicity, hence, explaining the failure of wortmannin to alter AA+Fe toxicity.

We investigated the possible role of phosphatases in the de-phosphorylation of AKT after exposure of E47 cells to AA+Fe in the presence or absence of LY294002. Specific cell-permeable inhibitors of serine/threonine phosphatases were used, okadaic acid for PP1C and

PP2A, and FK506 for PP2B. These inhibitors, at concentrations regularly used for cell studies and that didn't show significant toxicity by themselves (0-100 nM for okadaic acid, 0-20 μM for FK506), did not affect the toxicity of AA+Fe in the absence or presence of LY294002 (data not shown). Thus, stimulation of phosphatases such as PP1C, PP2A and PP2B by ROS produced from the treatment with AA+Fe does not appear to be responsible for the deactivation of AKT.

Hepatocyte studies.

Studies were performed to extend the observations made in CYP2E1-expressing HepG2 cells to non-transformed, intact, CYP2E1-expressing rat hepatocytes. Hepatocytes showed stable levels of CYP2E1 protein (assessed by western blot), and detectable CYP2E1 activity, assessed through metabolism of 7-MFC in situ (data not shown). Hepatocytes were cultured in MEM_{exps} as described in Materials and Methods. AA+Fe produced synergistic toxicity in intact hepatocytes (viability 99±6%, 84±4%, and 54±2 % with AA 25 μM alone, Fe-NTA 100 μM alone and the combination AA+Fe, respectively). Similar as in E47 cells, pre-incubation of intact hepatocytes with 50 μM LY294002 produced a decrease in cellular viability after exposure to 25 μM AA+ 100 μM Fe-NTA (viability 71±1%, 92±3%, and 54±2 % with AA 25 μM + Fe-NTA 100 μM, 50 μM LY294002 alone, and AA+Fe+50 μM LY294002, respectively). Intact hepatocytes pre-incubated with 50 μM LY294002 and further treated with AA+Fe for 4h showed lower levels of pAKT (pAKT/AKT ratio= 0.7) than intact hepatocytes incubated with AA+Fe alone (pAKT/AKT ratio= 1.0, data not shown).

Role of oxidative stress on cellular toxicity and AKT deactivation.

Oxidative stress and lipid peroxidation are the primary cause of cell death in this model of CYP2E1-dependent toxicity (Caro and Cederbaum, 2001; 2002). The next set of experiments (Fig 5) investigated if the decrease in phosphorylated AKT after AA+Fe treatment of E47 cells

JPET Fast Forward. Published on April 19, 2006 as DOI: 10.1124/jpet.106.102921
This article has not been copyedited and formatted. The final version may differ from this version.

depended on increased oxidative stress and lipid peroxidation. In panel A a representative western blot of phosphorylated AKT of lysates from E47 cells pre-incubated with α-tocopherol (αT), an effective liposoluble antioxidant, LY294002, or the combination of both, and further exposed to Fe-NTA (0-3h) is shown. As was presented in Fig 1A, the AA-loaded E47 cells treated with Fe-NTA for 3h showed a small decrease in phosphorylated AKT with respect to zero time controls; pre-incubation with LY294002 caused a further decrease in pAKT levels (Fig 5A). The decrease in pAKT by AA+Fe in the absence and presence of LY294002 was completely prevented by pre-incubation with α-tocopherol (Fig 5A). AA+Fe caused around 50% loss of viability in E47 cells, and this toxicity was further increased to a 80% loss of viability by pre-incubation with LY294002 (Fig 5B). α-Tocopherol completely prevented both AA+Fe- and AA+Fe+LY294002- induced toxicity (Fig 5B).

Effect of LY294002 on upstream mediators of AA/Fe toxicity in E47 cells.

We previously suggested that CYP2E1-dependent toxicity induced by AA+Fe is mediated through an increase in lipid peroxidation that triggers an increase in intracellular calcium, and activation of Ca^{2+}-dependent hydrolases such as calpain and PLA2 (Caro and Cederbaum, 2002; 2003). Considering that LY294002 increased AA+Fe toxicity, the possibility that LY294002 may affect upstream mediators of toxicity was investigated (Table 1). TBARS content, an index of lipid peroxidation, increased around 4-fold after AA+Fe treatment of E47 cells; the same increase in lipid peroxidation levels was observed in the presence of AA+Fe+LY294002 (Table 1). Intracellular calcium was measured by flow cytometry using fluo3 and gating for the PI negative, i.e. viable, E47 cells. AA+Fe caused a 2-fold increase in intracellular calcium; the same increase was detected in the presence of AA+Fe+LY294002. Release of pre-loaded ^{3}H-AA (a measurement of in situ PLA2 activity) increased from 9.3 to 14.6% after treatment with AA+Fe,

while in the presence of LY294002, a similar increase was detected. Calpain activation was evaluated by analyzing spectrin degradation products. Alpha-spectrin is cleaved by calpain to two fragments of molecular weights 150 and 145 kDa, and by caspase 3 to two fragments of 150 and 120 kDa. AA+Fe-treatment in E47 cells produced an increased cleavage of alpha-spectrin to the 145 kDa calpain-specific fragment (upper arrow), and the same pattern and intensity of cleavage was observed in the presence of LY294002. Practically no cleavage of alpha-spectrin to the caspase 3-specific 120 kDa fragment (lower arrow) was observed in the absence or presence of LY294002, suggesting cell death in this model is primarily necrosis not apoptosis (also reflected by cell swelling, formation of plasma membrane blebs, vacuolization of cytoplasm, early depletion of ATP, lack of DNA ladder formation and absence of caspase activation (Caro and Cederbaum, 2001). To further show that the AA+Fe toxicity in the presence of LY294002 was mainly necrosis, an annexin V/PI flow cytometry experiment was carried out. At early time points (2-3h), AA+Fe did not cause annexin V staining in the absence or presence of LY294002 whereas PI staining was elevated (data not shown). CYP2E1 activity in situ assessed through the oxidation of a specific fluorogenic substrate did not change by incubation with LY294002 (Table 1). These results suggest that the increased toxicity promoted by LY294002 is downstream of the CYP2E1-dependent oxidative stress and activation of calcium-dependent hydrolases.

Role of mitochondrial damage in AA+Fe-induced cytotoxicity.

We suggested that in AA+Fe-treated E47 cells, lipid peroxidation, intracellular calcium, calpain and PLA2 activity are events that converge on mitochondria, inducing a profound bioenergetic failure and a rapid necrotic cell death (Caro and Cederbaum, 2002; 2003). Considering the key role of mitochondrial damage in cytotoxicity, the effect of LY294002 on mitochondrial function in the presence of AA+Fe was studied. Mitochondrial damage is initially manifested by a

decrease in mitochondrial membrane potential followed by ATP depletion (Orrenius et al., 1996). Mitochondrial membrane potential was assessed by measuring potential-driven mitochondrial accumulation of rhodamine 123 by flow cytometry. Kinetic studies were done measuring the percentage of the M1 population (cells showing low rhodamine fluorescence, directly related to mitochondrial membrane potential) with time. E47 cells preincubated with LY294002 and treated with AA+Fe showed higher percentage of cells in the M1 fraction than cells treated only with AA+Fe at all time points evaluated (Fig 6A). Similar experiments were done with mitotracker orange instead of rhodamine123/PI. In this case, E47 cells preincubated with LY294002 and treated with AA+Fe showed higher percentage of cells in the M1 fraction (low mitotracker orange fluorescence, 27±1%) than cells treated only with AA+Fe (15±1%) after 3h of exposure to Fe-NTA (data not shown). Thus, using two different probes, LY294002 was shown to enhance the AA+Fe mediated decline in mitochondrial membrane potential. ATP content followed a similar trend: E47 cells exposed to AA+Fe showed an early decrease in ATP concentration that precedes the toxicity, and the decrease in ATP levels caused by AA+Fe was higher in the presence of LY294002 (Fig 6B).

The oxidative stress status of the cells was assessed through the intracellular oxidation of DCFH by ROS, and the levels of glutathione, the principal water soluble cellular antioxidant. DCFH oxidation was quantified in PI negative (i.e. viable) cells, thus assuring any change observed occurs before the onset of cell death. In AA+Fe-treated cells, a very early increase in DCFH fluorescence and decrease in total glutathione levels was observed. Cells treated with LY294002 and AA+Fe did not show major differences in DCFH oxidation and GSH levels with respect to cells treated with AA+Fe alone at all time points evaluated (Figs 6C and 6D). Thus, LY294002 is not modulating the AA+Fe+CYP2E1 generated oxidant stress.

Two major processes are likely candidates as mechanisms for a loss of mitochondrial membrane potential: non-specific damage to the inner mitochondrial membrane, or a more specific process, the mitochondrial permeability transition (MPT), due to the opening of the MPT pore (Susin et al., 1998). Inhibitors of the MPT such as the cyclophilin D inhibitor cyclosporine A, the ANT inhibitor bongkrekic acid, and fructose/trifluoperazine, a combination proven to provide a fairly specific inhibition of the MPT in iron-treated hepatocytes (Rauen et al., 2004) partially inhibited AA+Fe-induced toxicity in E47 cells (Fig 7A bars 1 to 8). The increased toxicity caused by treatment with AA+Fe in the presence of LY294002 was also blocked by fructose/trifluoperazine (Fig 7A last 4 bars). The decrease in mitochondrial membrane potential (reflected by an increase in the population of cells with low rhodamine fluorescence, M1 population) caused by AA+Fe in the absence or the more pronounced decrease in the presence of LY294002 was blocked by fructose/trifluoperazine (Fig 7B). Fructose/trifluoperazine did not significantly affect lipid peroxidation in AA+Fe-treated cells, or CYP2E1 activity in situ (data not shown), suggesting its effects were not mediated by an antioxidant mechanism.

Effect of adenoviral delivery of constitutively active AKT.

After AA-loading, E47 cells were infected with ADV-MyrAKT or ADV-LacZ. After 24h of infection, cells were exposed to Fe-NTA for 3h. Control cells were not exposed to AA or Fe-NTA, but were infected with adenovirus. Adenoviral expression of active AKT decreased the percentage of cells with low rhodamine 123 fluorescence (M1 population) caused by AA+Fe-treatment of E47 cells as compared to the ADV-LacZ controls (Fig 8A), suggesting a partial protection by active AKT against the mitochondrial impairment. Adenoviral expression of active AKT decreased the percentage of cells stained with PI (reflecting plasma membrane permeabilization) caused by AA+Fe-treatment of E47 cells as compared to the ADV-LacZ

controls (Fig 8B), suggesting a partial protection by active AKT against the cytotoxicity. The adenovirus-mediated expression of constitutively active AKT was confirmed by detecting the HA tag (Fig 8C) after 24h of infection.

We evaluated the effects of adenoviral myrAKT overexpression on upstream mediators of the AA+Fe toxicity pathway, CYP2E1 activity in situ, ROS levels, and Ca^{2+} levels. E47 cells infected with ADV-myrAKT did not show a significant change in CYP2E1 activity in situ, with respect to E47 cells infected with ADV-LacZ (data not shown). AA+Fe caused a significant increase in ROS and intracellular calcium levels in ADV-LacZ- infected E47 cells, to the same extent as in myrAKT-ADV-infected E47 cells (data not shown). Thus, the myrAKT-ADV was not affecting upstream mediators of AA+Fe toxicity, analogous to the lack of effect of LY294002 on these upstream mediators.

Possible downstream mediators of AKT action.

Possible targets of active AKT with relevance for mitochondrial protection are, among others, GSK-3β, bad, mTOR, and bcl-xl (Juhaszova et al., 2004; Hu and Sayeed, 2005). Immumoblots for GSK-3β and bad show that its phosphorylation levels (phosphorylated protein/total protein, associated with cell protection and viability) were not significantly affected by AA+Fe (data not shown). Control experiments showed that LY294002 inhibited phosphorylation of AKT and GSK3β by hepatocyte growth factor, thus validating that LY294002 was inhibiting AKT activity/function. Bcl-xl is an antiapoptotic member of the bcl-2 family. The protein levels of bcl-xL did not show significant changes with time in cells incubated with AA+Fe in the absence or presence of LY294002 (data not shown). The mammalian target of rapamycin (mTOR) is considered a critical player for cell signaling pathways from translational machinery, cell growth and metabolism to survival/ apoptosis in many cell types (Li et al., 2005). Phosphorylation of

mTOR may be triggered by activation of its upstream molecules PI3 kinase and Akt. We evaluated the possible role of mTOR in the protection against toxicity in AA+Fe-treated E47 cells. Rapamycin (up to 100 μM) did not affect the toxicity of AA+Fe in the absence or presence of LY294002 (data not shown). Immumoblots for mTOR show that its phosphorylation levels were not significantly affected by AA+Fe in the absence or presence of LY294002 (data not shown).

DISCUSSION

The following experimental evidence suggests that PI3 kinase/AKT is a survival pathway against CYP2E1 plus AA/Fe- dependent toxicity: a) treatment of E47 cells with AA+Fe, a CYP2E1-dependent model of cell death, is associated with an early decrease in AKT activation. AA+Fe produced an early deactivation of AKT in CYP2E1-expressing cells, but not in control cells that do not express any cytochrome P450, an event that paralleled toxicity; b) toxicity by AA+Fe, evaluated as plasma membrane permeabilization to propidium iodide, was inhibited by expression of active AKT; c) toxicity of AA+Fe in CYP2E1-expressing HepG2 cells was enhanced by inhibition of PI3 kinase/AKT. Inhibition of PI3 kinase/AKT was performed with structurally unrelated chemical inhibitors or siRNAs directed against AKT 1, 2 and 3, and was confirmed by AKT deactivation.

AKT deactivation required AA+Fe, and CYP2E1 overexpression. Without AA+Fe, or with AA+Fe in control non-P450 expressing HepG2 cells, no deactivation of AKT is observed. This requirement is linked to oxidative stress and lipid peroxidation, as α-tocopherol blocked the AA+Fe-induced AKT deactivation in E47 cells. Possible mechanisms may include PI3 kinase deactivation, activation of serine/threonine phosphatases which can dephosphorylate AKT directly (Luo et al., 2003), or specific oxidation of AKT by ROS that may modify phosphorylation sites. Phosphatase inhibitors such as okadaic acid (PP1C and PP2A inhibitor) or FK506 (PP2B inhibitor) did not affect the toxicity of AA+Fe in the absence or presence of LY294002, suggesting that okadaic acid/FK506-sensible phosphatases are not involved in the mechanisms of toxicity. The underlying mechanism for the decrease in AKT activation after AA+Fe depends on increased oxidative stress, but how oxidative stress is promoting deactivation of AKT requires additional investigation.

Several studies suggest that the MPT pore opening in mitochondria is a factor in the pathogenesis of necrotic cell death. According to this hypothesis, the opening of the MPT pore induces the uncoupling of mitochondria, ATP hydrolysis, and acceleration of the onset of cell death (Li et al., 2004). Cytotoxicity by AA+Fe+CYP2E1 was inhibited by several MPT inhibitors (Fig 7A). Also, toxicity was associated with early depletion of cellular ATP and a decrease in mitochondrial membrane potential, an effect that was inhibited by fructose/trifluoperazine. These results suggest that opening of the MPT pore is associated with mitochondrial impairment and cell death in our model. Overexpression of active AKT decreased the loss of mitochondrial membrane potential associated with AA+Fe in E47 cells and partially prevented toxicity, without affecting CYP2E1 acitivity, ROS levels, or intracellular calcium with respect to AA+Fe-treated E47 cells infected with a control adenovirus. This suggests that the protection afforded by active AKT is downstream of the CYP2E1-dependent oxidative stress and the increase in intracellular calcium. Inhibition of PI3K/AKT with LY294002 in AA+Fe-treated E47 cells produced increased cytotoxicity and a more pronounced loss of ATP and mitochondrial membrane potential, effects blocked by fructose/trifluoperazine. LY294002 did not significantly affect the Fe+AA-induced activation of PLA2 and calpain, the increase in oxidative stress indices such as lipid peroxidation, DCFH oxidation and depletion of GSH content, or CYP2E1 activity. Thus, the increased toxicity promoted by LY294002 is downstream of the CYP2E1-dependent oxidative stress and activation of calcium-dependent hydrolases. We suggest that AKT is partially preventing cell toxicity by AA+Fe+CYP2E1 through inhibition of the MPT pore opening and the loss of mitochondrial membrane potential and of ATP, since LY294002 potentiated the decline in mitochondrial membrane potential and ATP produced by AA+Fe whereas adenoviral expression of active AKT protected against this loss of mitochondrial

membrane potential and of ATP. This is a critical mechanistic aspect, because although in several systems AKT can mediate rescue from cell death, AKT can exert its effects upstream (Kennedy et al., 1999) or downstream (Zhou et al., 2000) of mitochondria.

CYP2E1 dependent toxicity in our model does not seem to depend on the protein levels or activation of bad, GSK-3β or bcl-xl, as we could not detect significant early changes in the levels or phosphorylation states of these proteins after AA+Fe treatment in the absence or presence of LY294002. Akt modulates energy homeostasis by maintaining the level of ATP in cells (Hahn-Windgassen et al., 2005). The effect of Akt on the generation of ATP occurs via an increase in glycolysis and oxidative phosphorylation, although the one or more exact mechanisms by which Akt affects these processes are not known (Hahn-Windgassen et al., 2005). Considering the effects of AKT activation and inhibition on ATP levels and mitochondrial membrane potential in our system, experiments evaluating the modulation of mitochondrial bioenergetics by AKT will be important to try to identify downstream mediators of AKT-dependent inhibition of mitochondrial damage in CYP2E1-expressing cells.

This work is the first report for a role of PI3 kinase/AKT in the protection against CYP2E1-dependent cell necrosis. Alcoholic liver disease is associated with CYP2E1 induction, and an increase in the number of necrotic and apoptotic liver parenchymal cells. Several reports in the literature suggest a role for PI3 kinase/AKT in the protection of liver cells against ethanol-induced toxicity. Chronic ethanol exposure activated caspase 3 in hepatocytes, and this was associated with reduced levels of PI3 kinase, AKT and increased levels of PTEN phosphatase. This suggests that chronic ethanol exposure impairs survival mechanisms in the liver because of inhibition of signaling through PI3 kinase and AKT and increased levels of PTEN (Yeon et al., 2003). Ethanol-exposed liver cells displayed a blunting of TNF-α induced AKT activation that

may account, in part, for the increased sensitivity of the mitochondria to bax-mediated damage (Pastorino et al., 2003). Considering induction of CYP2E1 by alcohol and the role of PI3 kinase/AKT in the protection against CYP2E1-dependent cytotoxicity, it is interesting to speculate that part of the decrease in PI3 kinase- mediated signaling in alcohol liver disease may be the result of CYP2E1 overexpression. In this regard, CYP2E1 overexpression in liver cells decreased the effects of insulin on AKT activation, and GSK-3 and FoxO1a phosphorylation (Schattenberg et al., 2005).

Figure 9 presents a scheme which summarizes results presented in this study. CYP2E1 generates ROS such as superoxide and H_2O_2, which in the presence of AA+Fe promotes lipid peroxidation. The products of lipid peroxidation (lipid hydroperoxides, malondialdehyde, 4-hydroxynonenal) cause: a) an increase in intracellular calcium, with a consequent activation of Ca^{2+} -dependent hydrolases PLA2 and calpain (Caro and Cederbaum, 2003), and b) deactivation of the AKT survival pathway. Each of these events negatively impact on the mitochondria causing a decline in the mitochondrial membrane potential and ATP levels, which results in cell toxicity. The decline in bioenergetic function resulting from the deactivation of the AKT pathway by AA+Fe is probably mediated by opening of the mitochondrial permeability transition pore, but does not appear to be mediated by changes in GSK3β, bad, bcl-xl or mTOR, and the exact target(s) regulated by AKT remains to be defined. LY294002 potentiates the toxicity of AA+Fe in E47 cells by causing a further deactivation of AKT. The deactivation of AKT by AA+Fe is downstream of CYP2E1, and CYP2E1 catalyzed lipid peroxidation, and is independent of the increase in intracellular calcium and activation of PLA2 and calpain. α-Tocopherol, which prevents the lipid peroxidation, prevents all the downstream events associated with the increased lipid peroxidation such as the increase in Ca^{2+} and PLA2 (Caro and Cederbaum, 2003), the

deactivation of AKT (Fig 5A) and the decline in mitochondrial membrane potential and ATP, and hence, prevents cell death.

REFERENCES

Albright C, da Costa KA, Craciunescu C, Klem E, Mar MH and Zeisel S (2005) Regulation of choline deficiency apoptosis by epidermal growth factor in CWSV-1 rat hepatocyes. *Cell Physiol Biochem* **15:**59-68.

Bilodeau M, Tousignant J, Ethier C, Rocheleau B, Raymond VA and Lapointe R (2004) Anti-apoptotic effect of insulin on normal hepatocytes in vitro and in vivo. *Apoptosis* **9:**609-617.

Cantley LC (2002) The phosphoinositide 3-kinase pathway. *Science* **296:**1655-1657.

Caro AA and Cederbaum AI (2001) Synergistic toxicity of iron and arachidonic acid in HepG2 cells overexpressing CYP2E1. *Mol Pharmacol* **60:**742-752.

Caro AA and Cederbaum AI (2002) Role of calcium and calcium-activated proteases in CYP2E1-dependent toxicity in HEPG2 cells. *J Biol Chem* **277:**104-113.

Caro AA and Cederbaum AI (2003) Role of phospholipase A2 activation and calcium in CYP2E1-dependent toxicity in HepG2 cells. *J Biol Chem* **278:**33866-33877.

Caro AA and Cederbaum AI (2004) Oxidative stress, toxicology, and pharmacology of CYP2E1. *Annu Rev Pharmacol Toxicol* **44:**27-42.

Chang HC, Tsai LH, Chuang LY and Hung WC (2001) Role of AKT kinase in sphingosine-induced apoptosis in human hepatoma cells. *J Cell Physiol* **188:**188-193.

Chen Q and Cederbaum AI (1998) Cytotoxicity and apoptosis produced by cytochrome P450 2E1 in Hep G2 cells. *Mol Pharmacol* **53:**638-648.

Cross MJ, Stewart A, Hodgkin MN, Kerr DJ and Wakelam MJ (1995) Wortmannin and its structural analogue demethoxyviridin inhibit stimulated phospholipase A2 activity in Swiss 3T3 cells. Wortmannin is not a specific inhibitor of phosphatidylinositol 3-kinase. *J Biol Chem* **270:**25352-25355.

Dan HC, Sun M, Kaneko S, Feldman RI, Nicosia SV, Wang HG, Tsang BK and Cheng JQ (2004) Akt phosphorylation and stabilization of X-linked inhibitor of apoptosis protein (XIAP). *J Biol Chem* **279:**5405-5412.

Datta SR, Brunet A and Greenberg ME (1999) Cellular survival: a play in three Akts. *Genes Dev* **13:**2905-2927.

Fruman DA, Mauvais-Jarvis F, Pollard DA, Yballe CM, Brazil D, Bronson RT, Kahn CR and Cantley LC (2000) Hypoglycaemia, liver necrosis and perinatal cell death in mice lacking all isoforms of phosphoinositide 3-kinase p85α. *Nat Genet* **26:**379-382.

Ghosal A, Hapangama N, Yuan Y, Lu X, Horne D, Patrick JE and Zbaida S (2003) Rapid determination of enzyme activities of recombinant human cytochromes P450, human liver microsomes and hepatocytes. *Biopharm Drug Dispos* **24:**375-84.

Harada N, Hatano E, Koizumi N, Nitta T, Yoshida M, Yamamoto N, Brenner DA and Yamaoka Y (2004) AKT activation protects rat liver from ischemia/reperfusion injury. *J Surg Res* **121:**159-170.

Hahn-Windgassen A, Nogueira V, Chen CC, Skeen JE, Sonenberg N and Hay N (2005) Akt activates the mammalian target of rapamycin by regulating cellular ATP level and AMPK activity. *J Biol Chem* **280:**32081-32089.

Hu Z and Sayeed MM (2005) Activation of PI3-kinase/PKB contributes to delay in neutrophil apoptosis after thermal injury. *Am J Physiol Cell Physiol* **288:**C1171-C1178.

Izuishi K, Fujiwara M, Hossain MA, Usuki H and Maeta H (2003) Significance of phosphoinositide 3-kinase pathway on ischemic preconditioning followed by ischemia reperfusion in mice liver. *Transplant Proc* **35:**132-133.

Juhaszova M, Zorov DB, Kim SH, Pepe S, Fu Q, Fishbein KW, Ziman BD, Wang S, Ytrehus K, Antos CL, Olson EN and Sollott SJ (2004) Glycogen synthase kinase-3beta mediates convergence of protection signaling to inhibit the mitochondrial permeability transition pore. *J Clin Invest* **113:**1535-1549.

Kang KW, Ryu JH and Kim SG (2001a) Activation of phosphatidylinositol 3-kinase by oxidative stress leads to the induction of microsomal epoxide hydrolase in H4IIE cells. *Toxicol Lett* **121:**191-197.

Kang KW, Cho MK, Lee CH and Kim SG (2001b) Activation of phosphatidylinositol 3-kinase and Akt by tert-butylhydroquinone is responsible for antioxidant response element-mediated rGSTA2 induction in H4IIE cells. *Mol Pharmacol* **59:**1147-1156.

Kennedy SG, Kandel ES, Cross TK and Hay N (1999) Akt/Protein kinase B inhibits cell death by preventing the release of cytochrome c from mitochondria. *Mol Cell Biol* **19:**5800–5810.

Kuo, ML, Chuang SE, Lin MT and Yang SY (2001) The involvement of PI3-K/Akt dependent up-regulation of Mcl-1 in the prevention of apoptosis of Hep3B cells by interleukin-6. *Oncogene* **20:**677-685.

Lee TK, Man K, Ho JW, Sun CK, Ng KT, Wang XH, Wong YC, Ng IO, Xu R and Fan ST (2004) FTY720 induces apoptosis of human hepatoma cell lines through PI3-K-mediated AKT dephosphorylation. *Carcinogenesis* **25:**2397-2405.

Leng J, Han C, Demetris AJ, Michalopoulos GK and Wu T (2003) Cyclooxygenase-2 promotes hepatocellular carcinoma cell growth through AKT activation: evidence for Akt inhibition in celecoxib-induced apoptosis. *Hepatology* **38:**756-768.

Li S, Fang CX, Aberle NSII, Ren BH, Ceylan-Isik AF and Ren J (2005) Inhibition of PI-3 kinase/Akt/mTOR, but not calcineurin signaling, reverses insulin-like growth factor I-induced protection against glucose toxicity in cardiomyocyte contractile function. *J Endocrinol* **186:** 491-503.

Li Y, Johnson N, Capano M, Edwards M and Crompton M (2004) Cyclophilin-D promotes the mitochondrial permeability transition but has opposite effects on apoptosis and necrosis. *Biochem J* **383:**101-109.

Luo HR, Hattori H, Hossain MA, Hester L, Huang Y, Lee-Kwon W, Donowitz M, Nagata E and Snyder SH (2003) AKT as a mediator of cell death. *Proc Nat Acad Sci USA* **100:**11712-11717.

Orrenius S, Ankarcrona M and Nicotera P **(**1996) Mechanisms of calcium-related cell death. *Adv Neurol* **71:**137-151.

Pastorino JG, Shulga N and Hoek JB (2003) TNF-alpha-induced cell death in ethanol-exposed cells depends on p38 MAPK signaling but is independent of Bid and caspase-8. *Am J Physiol Gastrointest Liver Physiol* **285:**G503-G516.

Rauen U, Petrat F, Sustmann R and de Groot H (2004) Iron-induced mitochondrial permeability transition in cultured hepatocytes. *J Hepatol* **40:**607-615.

Sautin, YY, Crawford JM and Svetlov SI (2001) Enhancement of survuival by LPA via Erk1/Erk2 and PI3 kinase/AKT pathways in a murine hepatocyte cell line. *Am J Physiol Cell Physiol* **281:**C2010-C2019.

Schattenberg JM, Wang Y, Singh R, Rigoli RM and Czaja M (2005) Hepatocyte CYP2E1 overexpression and steatohepatitis lead to impaired hepatic insulin signaling. *J Biol Chem* **280:**9887-9894.

Schulze-Bergkamen H, Brenner D, Krueger A, Suess D, Fas SC, Frey CT, Dax A, Zink D, Buchler, P, Muller M and Krammer PH (2004) Hepatocyte growth factor induces Mcl-1 in primary human hepatocytes and inhibits CD95-mediated apoptosis via AKT. *Hepatology* **39:**645-654.

Susin SA, Zamzami N and Kroemer G (1998) Mitochondria as regulators of apoptosis: doubt no more. *Biochim Biophys Acta* **1366:**151-165.

Tietze F. (1969) Enzymic method for quantitative determination of nanogram amounts of total and oxidized glutathione: Applications to mammalian blood and other tissues. *Anal. Biochem.* **27:**502-522.

Wu D and Cederbaum AI (2003) Role of p38 MAPK in CYP2E1-dependent arachidonic acid toxicity. *J Biol Chem* **278:**1115-1124.

Yeon JE, Califano S, Xu J, Wands JR and de la Monte SM (2003) Potential role of PTEN phosphatase in ethanol-impaired survival signaling in the liver. *Hepatology* **38:**703-714.

Zangar RC, Davydov DR and Verma S. (2004) Mechanisms that regulate production of reactive oxygen species by cytochrome P450. *Toxicol Appl Pharmacol* **199:**316-331.

Zhou H, Li XM, Meinkoth J and Pittman RN (2000) Akt regulates cell survival and apoptosis at a postmitochondrial level. *J Cell Biol* **151:**483–494.

FOOTNOTES

This study was supported by USPHS grant AA 06610 from the National Institute on Alcohol Abuse and Alcoholism.

LEGENDS FOR FIGURES

Figure 1. AKT deactivation in E47 cells exposed to AA+Fe. (A) E47 cells were loaded with 5 μM AA for 12h, and further exposed to 25 μM Fe-NTA for up to 3h as described in Materials and Methods (AA+Fe, left panel), or were incubated without AA or Fe-NTA, but in the presence of vehicle (0.1%DMSO) for up to 3h, following the same protocol (Vehicle, right panel). At the indicated time points, protein extracts were collected, resolved by SDS/PAGE and immunoblotted with an antibody against phosphoAKT (Thr308). The membranes were stripped, and re-probed with an antibody against total AKT. After quantification of the bands, the ratio of pAKT over total AKT was calculated (number in parenthesis below the blots, standard error< 10%). (B) The same procedure was done as in (A), but using 10 μM LY294002 (stock solution x1000 in DMSO), in the presence or absence of AA+Fe. (C) C34 cells were loaded with 5 μM AA for 12h, and further exposed to 25 μM Fe-NTA for up to 3h as described in Materials and Methods, in the absence (AA+Fe) or presence of 10 μM LY294002 (stock solution x1000 in DMSO) (AA+Fe + LY294002). Western blots were performed as described in (A).

* Significantly different ($p<0.05$) with respect to zero time controls. One representative experiment out of 3 is shown.

Figure 2. Cytotoxicity in E47 cells exposed to AA+Fe. (A) E47 cells were loaded with 5 μM AA for 12h, and further exposed to 25 μM Fe-NTA for up to 3h as described in Materials and Methods, in the presence of vehicle (0.1% DMSO) (black circles) or 10 μM LY294002 (black squares). Control cells were incubated following the same general protocol, in the absence of AA or Fe-NTA, but in the presence of vehicle (white circles), or 10 μM LY294002 (white squares). Cytotoxicity was evaluated by the MTT reduction assay. (B) The same experiment as in (A) was performed, using C34 cells instead of E47 cells. (C) AA+Fe toxicity in E47 cells was examined

by phase-contrast photomicrography. E47 cells were incubated without AA/Fe (left column) or with 5 μM AA+25 μM Fe-NTA (right column). After addition of Fe-NTA or buffer, the cells were incubated for 2h before the analysis. The preincubation was performed with vehicle (0.1%DMSO) or 10 μM LY294002 (stock x1000 in DMSO).

* Significantly different ($p<0.05$) with respect to cells incubated in the same conditions, without AA+Fe. # Significantly different ($p<0.05$) with respect to cells incubated in the same conditions, without LY294002.

Figure 3. Efect of different PI3 kinase/AKT inhibitors on cytotoxicity and AKT activation in AA+Fe-treated E47 cells. In every case, E47 cells were first incubated with 5 μM AA following the general protocol described in Materials and Methods; control cells were not exposed to AA. Cells were preincubated with the different inhibitors for 1h prior to the addition of Fe-NTA (for AA-treated cells) or buffer (for controls). After 3h, viability was assessed by the MTT method. AKT activation in AA+Fe-treated E47 cells after 2h of incubation in the absence (-) or presence (+) of the corresponding inhibitor was evaluated by western blots of the protein extracts. (A) AKT inhibitor IV was used in a concentration range of 0.25-2 μM (viability assay), or at a concentration of 2 μM (western blot). (B) Deguelin was used in a concentration range of 0.5-10 μM (viability assay), or at a concentration of 10 μM (western blot). (C) siRNA against AKT1/2/3 was used at a concentration of 10 nM (viability assay and western blot); control experiments were performed with a non-targeting siRNA at 10 nM. (D) Wortmannin was used in a concentration range of 0.1-10 μM (viability assay), or at a concentration of 10 μM (western blot).

JPET Fast Forward. Published on April 19, 2006 as DOI: 10.1124/jpet.106.102921
This article has not been copyedited and formatted. The final version may differ from this version.

* Significantly different ($p<0.05$) with respect to cells incubated in the same conditions, without AA+Fe. # Significantly different ($p<0.05$) with respect to cells incubated in the same conditions, without AKT inhibitor.

Figure 4. Effect of wortmannin on AA+Fe-activated ^{3}HAA release. E47 cells were preloaded with 2 μM AA + 0.2 μCi/mL ^{3}HAA for 12h. After washing, cells were incubated with wortmannin (0.1-10 μM) or 100 μM quinacrine. After 1h, buffer or 25 μM Fe-NTA was added to each well, and ^{3}HAA release was evaluated after 3h as described in Materials and Methods.

* Significantly different ($p<0.05$) with respect to cells incubated in the same conditions, without Fe-NTA. # Significantly different ($p<0.05$) with respect to cells incubated in the same conditions, without any inhibitor.

Figure 5. Effect of α-tocopherol on cytotoxicity and AKT activation in AA+Fe-treated E47 cells. (A) E47 cells were preloaded with 5 μM AA, and preincubated with either 50 μM α-tocopherol (αT) or 10 μM LY294002 (LY) or the combination of 50 μM α-tocopherol+10 μM LY294002 (αT+LY) for 1h. Cells were immediately collected for western blot analysis of phosphoAKT (0h results), or incubated with 25 μM Fe-NTA for 3h before collection of protein samples for western blot. The ratio of pAKT over total AKT was calculated (number in parenthesis below the blots, standard error< 10%).

* Significantly different ($p<0.05$) with respect to cells incubated in the same conditions, at 0h. # Significantly different ($p<0.05$) with respect to cells incubated in the same conditions, without LY294002. @ Significantly different ($p<0.05$) with respect to cells incubated in the same conditions, without α-tocopherol.

(B) E47 cells were preloaded with 5 μM AA and either exposed to 25 μM Fe-NTA for 3h (Fe+AA), or left untreated. Preincubation was performed with 50 μM α-tocopherol (αT) or 10

μM LY294002 (LY) or the combination of 50 μM α-tocopherol+10 μM LY294002 (LY+αT). Viability was assessed by the MTT reduction assay.

* Significantly different ($p<0.05$) with respect to cells incubated in the same conditions, without AA+Fe. # Significantly different ($p<0.05$) with respect to cells incubated in the same conditions, without LY294002. @ Significantly different ($p<0.05$) with respect to cells incubated in the same conditions, without α-tocopherol.

Figure 6. Effect of AA+Fe and PI3 kinase inhibition on mitochondrial function in CYP2E1-expressing HepG2 cells. (A) E47 cells were either exposed to vehicle alone (white circles), 5 μM AA+25 μM Fe-NTA + vehicle (black circles), 10 μM LY294002 alone (white squares), or 5 μM AA+25 μM Fe-NTA + 10 μM LY294002 (black squares). After a toxicity phase of 1 to 3h, mitochondrial membrane potential was monitored by flow cytometry using rhodamine 123. The percentage of the cell population in the M1 fraction (low rhodamine 123 fluorescence) is represented versus time.

* Significantly different ($p<0.05$) with respect to cells incubated in the same conditions, without AA+Fe. # Significantly different ($p<0.05$) with respect to cells incubated in the same conditions, without LY294002.

(B) ATP content was monitored at several times during the toxicity phase (0-3h) as described in (A).

* Significantly different ($p<0.05$) with respect to cells incubated in the same conditions, without AA+Fe. # Significantly different ($p<0.05$) with respect to cells incubated in the same conditions, without LY294002.

(C and D) E47 cells were exposed to 5 μM AA+25 μM Fe-NTA (AA+Fe) or 5 μM AA+25 μM Fe-NTA + 10 μM LY294002 (AA+Fe+LY). After a toxicity phase of 0-3h, DCFH fluorescence

in PI negative cells (C) or glutathione content (D) was evaluated as described in Materials and Methods. * Significantly different ($p<0.05$) with respect to cells incubated in the same conditions, at time=0h.

Figure 7. Modulation of cytotoxicity and mitochondrial membrane potential by MPT inhibitors. E47 cells were either exposed to 5 μM AA + 25 μM Fe-NTA (+AA/Fe) or left untreated (-AA/Fe). Cells were preincubated for 1h with either 50 μM bongkrekic acid, or 2 μg/mL cyclosporine A, or 10 mM fructose+5 μM trifluoperazine (fructose/TFP), or 10 μM LY294002, or the combination fructose/trifluoperazine+LY294002. (A) Viability was assessed after a 2h toxicity phase as described under Materials and Methods. (B)The percentage of cells exhibiting low rhodamine 123 fluorescence (M1 population) was evaluated by flow cytometry.

* Significantly different ($p<0.05$) with respect to cells incubated in the same conditions, without AA+Fe. # Significantly different ($p<0.05$) with respect to cells incubated in the same conditions, without any inhibitor. @ Significantly different ($p<0.05$) with respect to cells incubated in the same conditions, without fructose/trifluoperazine.

Figure 8. Constitutively active AKT partially protects CYP2E1-expressing HepG2 cells from AA+Fe-induced cytotoxicity. E47 cells were either exposed to 5 μM AA + 25 μM Fe-NTA (+AA/Fe) or left untreated (-AA/Fe). Cells were infected with ADV-MyrAKT or ADV-LacZ as described under Materials and Methods. (A) The percentage of cells exhibiting low rhodamine 123 fluorescence (M1 population) was evaluated by flow cytometry after a 3h toxicity phase. (B) The percentage of cells exhibiting PI staining was evaluated by flow cytometry after a 3h toxicity phase. (C) The HA-tagged myrAKT was detected by western blotting using anti-HA antibody in whole extracts at 24h after ADV-MyrAKT infection. Control cells were infected with ADV-LacZ.

* Significantly different ($p<0.05$) with respect to cells incubated in the same conditions, without AA+Fe. # Significantly different ($p<0.05$) with respect to cells incubated in the same conditions, without ADV-myrAKT.

Figure 9. Scheme for the pathway for AA+Fe toxicity in E47 cells. Please see text for discussion.

JPET Fast Forward. Published on April 19, 2006 as DOI: 10.1124/jpet.106.102921
This article has not been copyedited and formatted. The final version may differ from this version.

Table 1

Effect of AA+Fe, and inhibition of PI3 kinase, on upstream mediators of toxicity in E47 cells. E47 cells were either loaded with 5 μM AA for 12h or left untreated. After washing, cells were preincubated for 1h with 10 μM LY294002, or with an equivalent amount of vehicle (0.1%DMSO). Following this, AA-loaded cells were incubated with Fe-NTA for 2h, while non-loaded cells received buffer. TBARS content, intracellular calcium, PLA2 activity in situ, calpain activation, and CYP2E1 activity in situ were assessed as described under Materials and Methods. Arrows loacalize the 145 kDa calpain-specific fragment of α-spectrin (upper arrow), and the 120 kDa caspase 3-specific fragment (lower arrow).

Treatment	TBARS (nmol/mg)	$[Ca^{2+}]_i$ (AU)	PLA2 (% ^{3}HAA release)	Calpain (SDPs)	CYP2E1 (AU)
Vehicle 2h	0.08±0.04	1.0	9.3±1.0	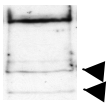	22±5
AA+Fe+vehicle 2h	0.33±0.05	2.1±0.1	14.6±1.7	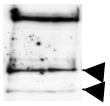	-
LY294002 2h	0.08±0.04	0.9±0.1	8.9±0.3	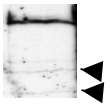	18±3
AA+Fe+LY294002 2h	0.33±0.05	1.7±0.2	13.9±0.6	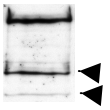	-

JPET Fast Forward. Published on April 19, 2006 as DOI: 10.1124/jpet.106.102921
This article has not been copyedited and formatted. The final version may differ from this version.

Figure 1

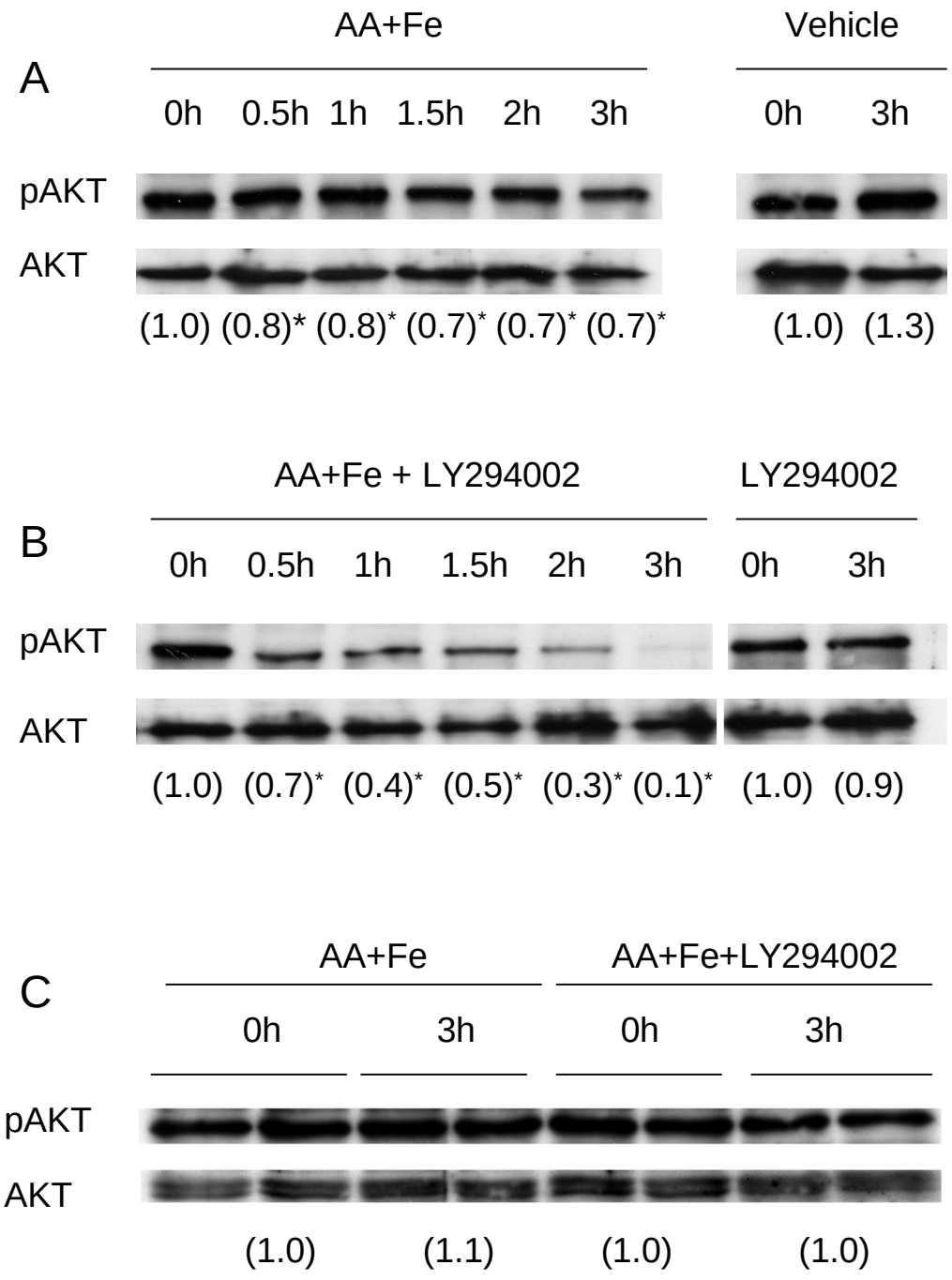

Figure 2

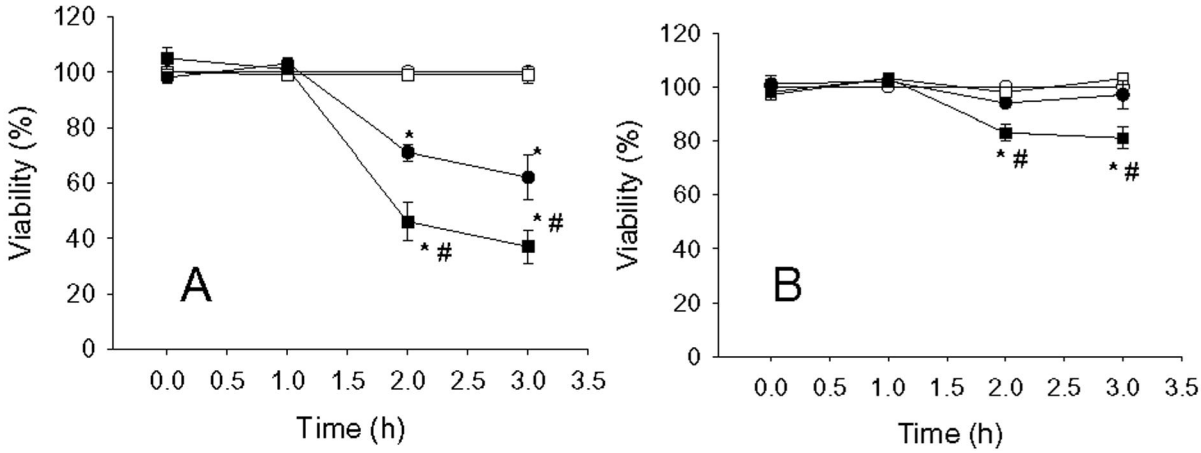
120
100
80
60
40
20
0
Viability (%)
A
0.0 0.5 1.0 1.5 2.0 2.5 3.0 3.5
Time (h)
B
C
Vehicle
AA+Fe+vehicle
10 uM LY294002
AA+Fe + 10 uM LY294002

JPET Fast Forward. Published on April 19, 2006 as DOI: 10.1124/jpet.106.102921
This article has not been copyedited and formatted. The final version may differ from this version.

Figure 3

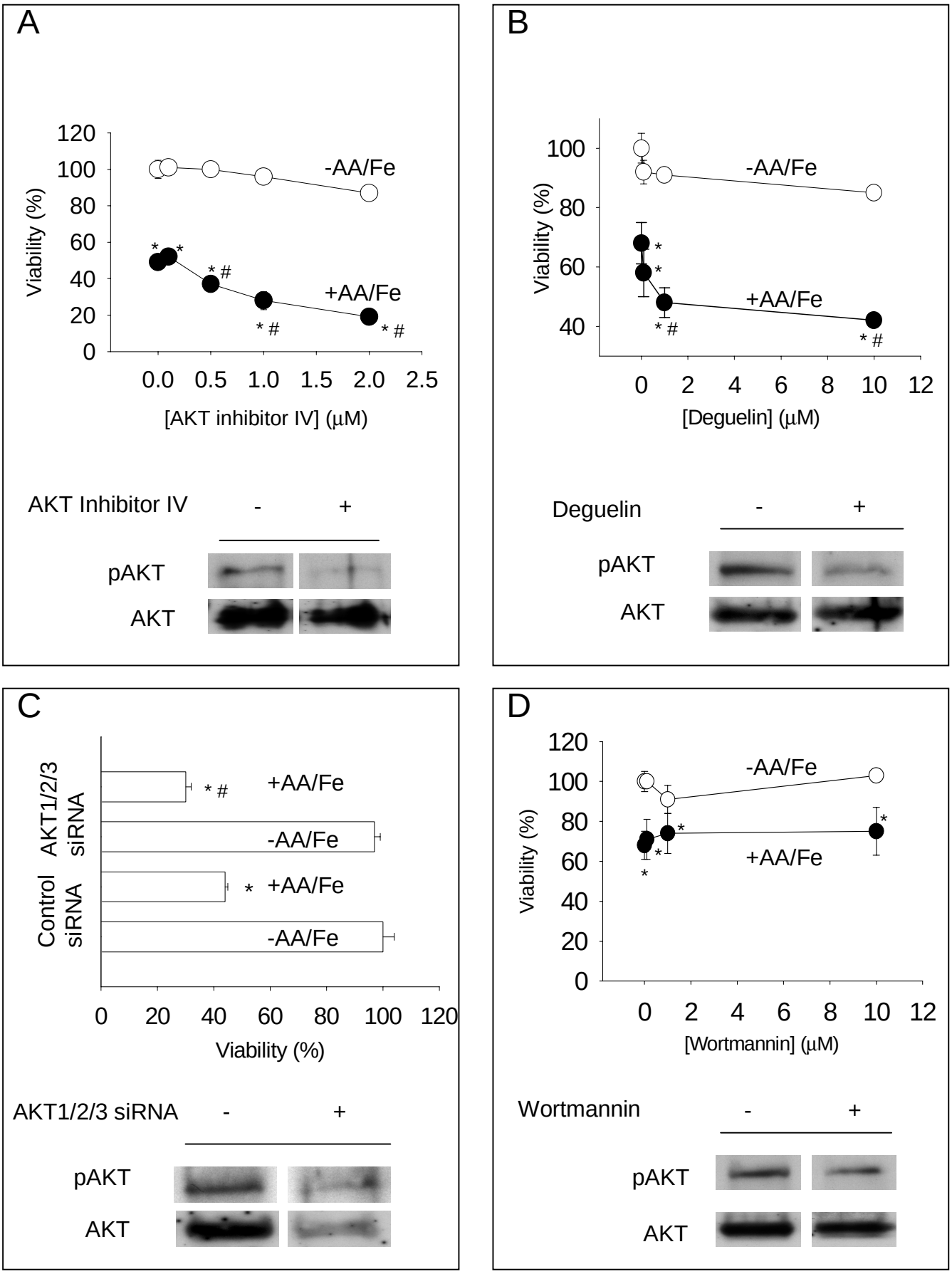

JPET Fast Forward. Published on April 19, 2006 as DOI: 10.1124/jpet.106.102921
This article has not been copyedited and formatted. The final version may differ from this version.

Figure 4

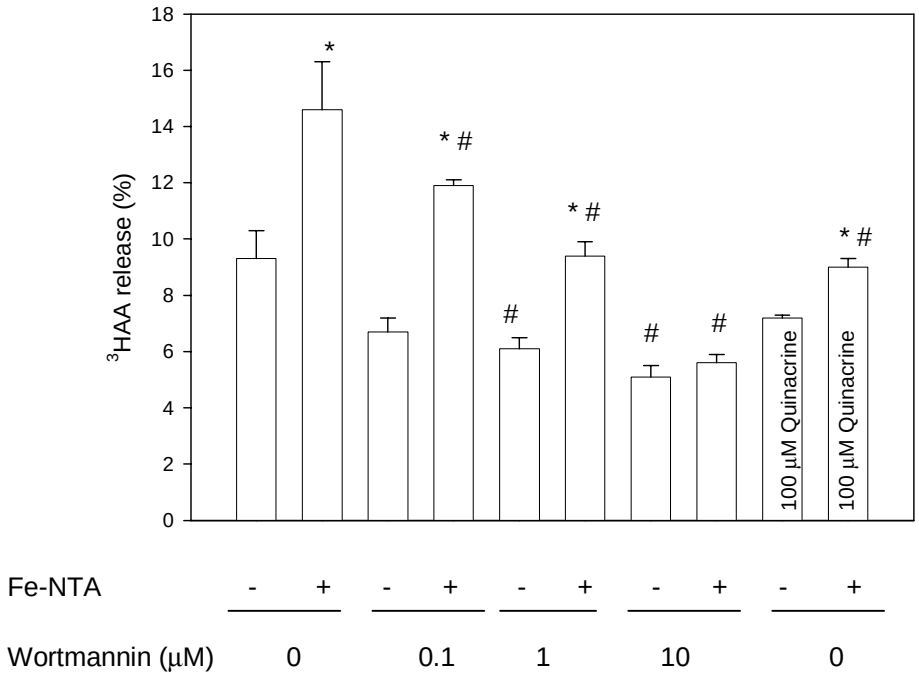

JPET Fast Forward. Published on April 19, 2006 as DOI: 10.1124/jpet.106.102921
This article has not been copyedited and formatted. The final version may differ from this version.

Figure 5

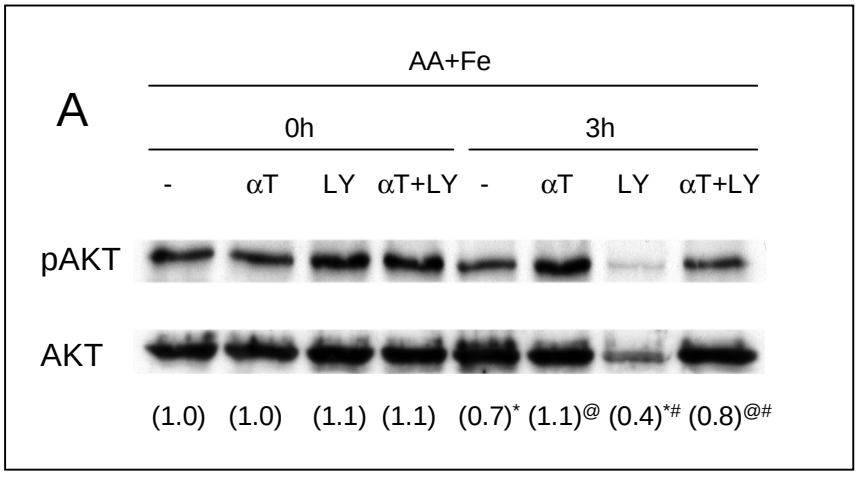

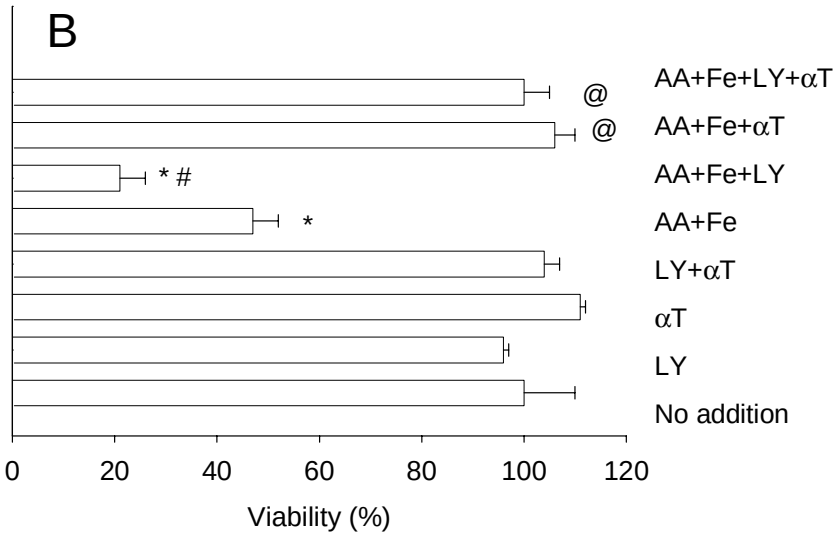

JPET Fast Forward. Published on April 19, 2006 as DOI: 10.1124/jpet.106.102921
This article has not been copyedited and formatted. The final version may differ from this version.

Figure 6

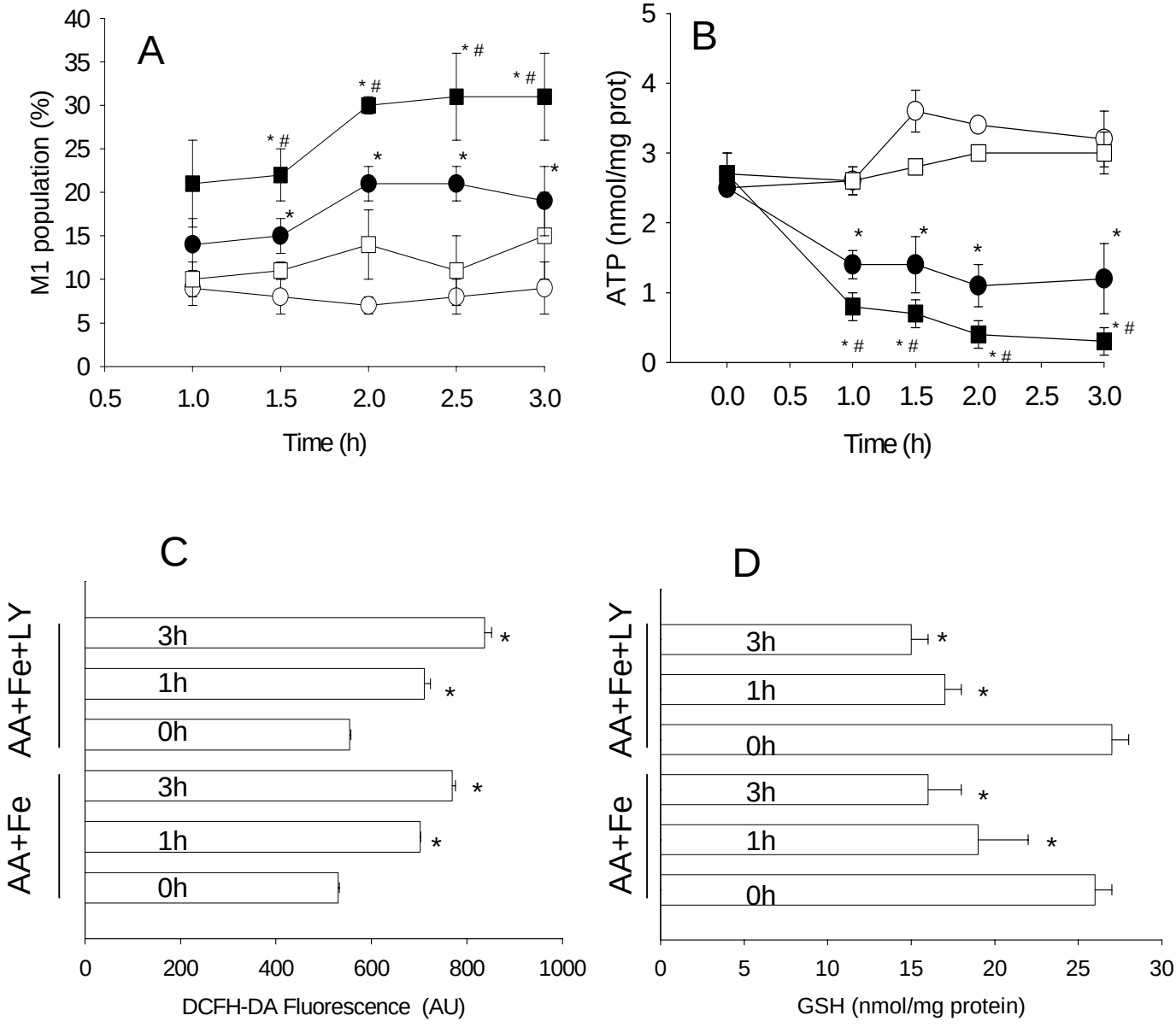

JPET Fast Forward. Published on April 19, 2006 as DOI: 10.1124/jpet.106.102921
This article has not been copyedited and formatted. The final version may differ from this version.

Figure 7

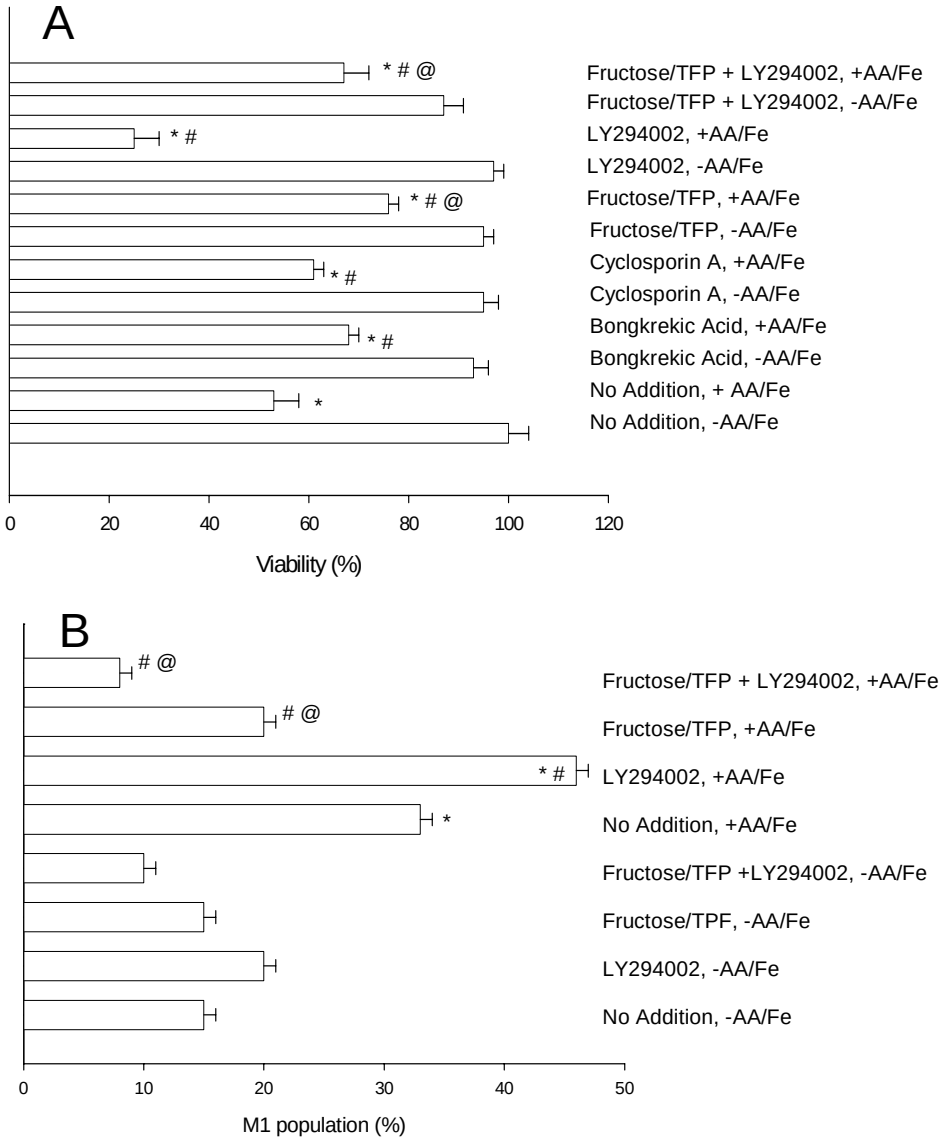

JPET Fast Forward. Published on April 19, 2006 as DOI: 10.1124/jpet.106.102921
This article has not been copyedited and formatted. The final version may differ from this version.

Figure 8

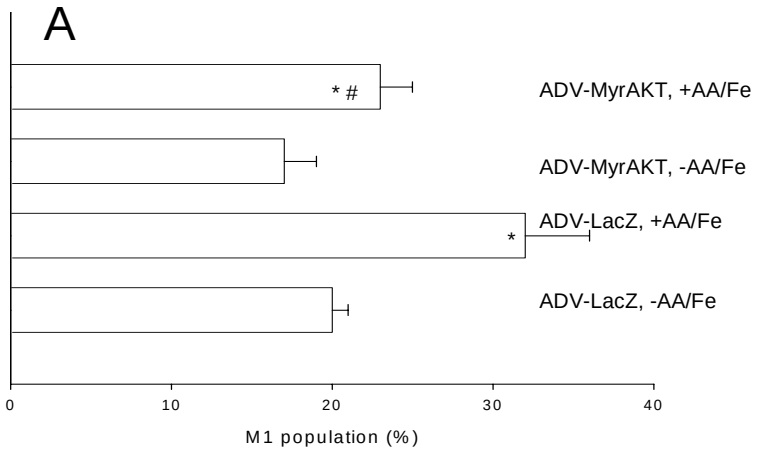

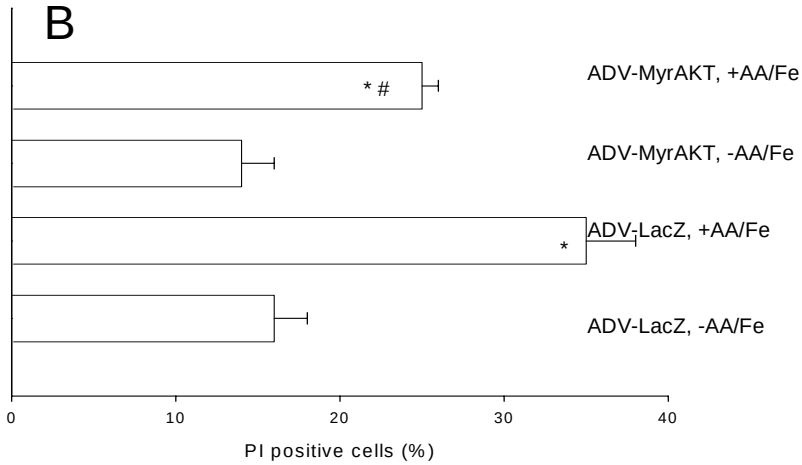

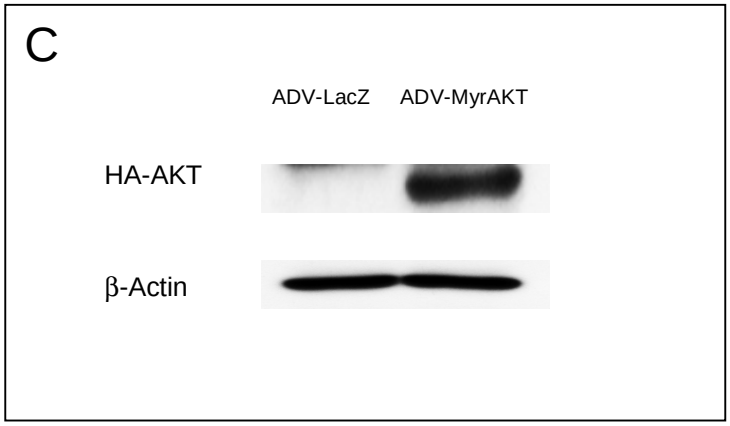

JPET Fast Forward. Published on April 19, 2006 as DOI: 10.1124/jpet.106.102921
This article has not been copyedited and formatted. The final version may differ from this version.

Figure 9